Draft version April 27, 2010
Preprint typeset using LaTeX style emulateapj v. 11/10/09

UNCERTAINTIES IN THE νp-PROCESS: SUPERNOVA DYNAMICS VERSUS NUCLEAR PHYSICS

Shinya Wanajo[1, 2], Hans-Thomas Janka[2], and Shigeru Kubono[3]

Draft version April 27, 2010

ABSTRACT

We examine how the uncertainties involved in supernova dynamics as well as in nuclear reactions affect the νp-process in the neutrino-driven winds of core-collapse supernovae. For the supernova dynamics, we find that the wind-termination by the preceding outgoing supernova ejecta, as well as the electron fraction at the onset of the νp-process, $Y_{\mathrm{e},3}$ (at 3×10^9 K), plays a crucial role. The wind-termination within the temperature range of $(1.5 - 3) \times 10^9$ K greatly enhances the efficiency of the νp-process. This implies that the early wind phase when the innermost layer of the preceding supernova ejecta is still $\sim 200 - 1000$ km from the center is most relevant to the p-nuclei production. The outflows with $Y_{\mathrm{e},3} = 0.50 - 0.60$ result in the production of the p-nuclei up to $A = 108$ (^{108}Cd) with interesting amounts, which fill the gap that cannot be accounted for by the γ-process scenario. Furthermore, the p-nuclei up to $A = 152$ (^{152}Gd) can be produced if $Y_{\mathrm{e},3} = 0.65$ is achieved. For the nuclear reactions, we test the sensitivity to the rates relevant to the breakout from the pp-chain region (triple-α, $^7\mathrm{Be}(\alpha,\gamma)^{11}\mathrm{C}$, and $^{10}\mathrm{B}(\alpha,p)^{13}\mathrm{C}$), and to the (n,p) rates on some iron-group nuclei (^{56}Ni, ^{60}Zn, and ^{64}Ge). We find that a small variation of triple-α as well as of $^{56}\mathrm{Ni}(n,p)^{56}\mathrm{Co}$ leads to a substantial change in the p-nuclei production, although the others also have non-negligible effects.

Subject headings: nuclear reactions, nucleosynthesis, abundances — stars: abundances — stars: neutron — supernovae: general

1. INTRODUCTION

The astrophysical origin of the proton-rich isotopes of heavy elements (p-nuclei) is not fully understood. The most successful model to date, that is, the photodissociation of pre-existing neutron-rich isotopes (γ-process) in the oxygen-neon layer of core-collapse supernovae, cannot explain the production of some lighter p-nuclei including ^{92,94}Mo and ^{96,98}Ru (e.g., Prantzos et al. 1990; Rayet et al. 1995; Hayakawa et al. 2008). The recent discovery of a new nucleosynthetic process, the νp-process, has dramatically changed this difficult situation (Fröhlich et al. 2006a,b; Pruet et al. 2006; Wanajo 2006). In the early neutrino-driven winds of core-collapse supernovae, $\bar{\nu}_e$ capture on free protons gives rise to a tiny amount of free neutrons in the proton-rich matter. These neutrons induce the (n, p) reactions on the β^+-waiting point nuclei along the classical rp-process path (^{64}Ge, ^{68}Se, and ^{72}Kr), which bypass these nuclei (with the β^+-decay half-lives of 1.06 min, 35.5 s, and 17.1 s, respectively). Wanajo (2006) has shown that the p-nuclei up to $A \sim 110$, including ^{92,94}Mo and ^{96,98}Ru, can be produced by the νp-process in the neutrino-driven winds within reasonable ranges of the model parameters.

All the recent hydrodynamic studies of core-collapse supernovae with neutrino transport taken into account suggest that the bulk of early supernova ejecta is proton rich (Janka, Buras, & Rampp 2003; Liebendörfer et al. 2003; Buras et al. 2006; Kitaura, Janka, & Hillebrandt 2006; Fischer et al. 2009; Hüdepohl et al. 2009). This supports the νp-process taking place in the neutrino-driven winds of core-collapse supernovae. However, different works end up with somewhat different outcomes. Fröhlich et al. (2006a) showed that the p-nuclei up to $A \sim 80$ were produced with the one-dimensional, *artificially* induced explosion model of a $20M_\odot$ star, while Pruet et al. (2006) obtained up to $A \sim 100$ with the two-dimensional, *artificially* induced explosion model of a $15M_\odot$ star. On the contrary, Wanajo et al. (2009) found no contribution of the νp-process to the production of p-nuclei at least within the first 1 second of the wind phase with the one-dimensional, *self-consistently* exploding model of a $9M_\odot$ star (electron-capture supernova, Kitaura, Janka, & Hillebrandt 2006). These diverse outcomes indicate that the νp-process is highly sensitive to the physical conditions of neutrino-driven winds.

Besides the supernova conditions, there could be also large uncertainties in some key nuclear rates, in particular of (n, p) reactions, because no attention was paid to neutron capture reactions on proton-rich nuclei before the discovery of the νp-process. Uncertainties in some reactions relevant to the breakout from the pp-chain region ($Z < 6$), which affect the proton-to-seed ratio at the onset of νp-processing, might also influence the nucleosynthetic outcomes.

Our goal in this paper is to examine how the variations of supernova conditions as well as of some nuclear reactions influence the global trend of the νp-process, such as the maximum overproduction and largest mass number of the synthesized p-nuclei. A semi-analytic neutrino-driven wind model and an up-to-date reaction network code are used for this purpose (§ 2). We take the wind-termination radius (or temperature), the neutrino luminosity, the neutron-star mass, and the electron fraction as the key parameters of supernova conditions (§ 3).

[1] Technische Universität München, Excellence Cluster Universe, Boltzmannstr. 2, D-85748 Garching, Germany; shinya.wanajo@universe-cluster.de
[2] Max-Planck-Institut für Astrophysik, Karl-Schwarzschild-Str. 1, D-85748 Garching, Germany; thj@mpa-garching.mpg.de
[3] Center for Nuclear Study, University of Tokyo, RIKEN Campus, 2-1 Hirosawa, Wako, Saitama 351-0198, Japan; kubono@cns.s.u-tokyo.ac.jp

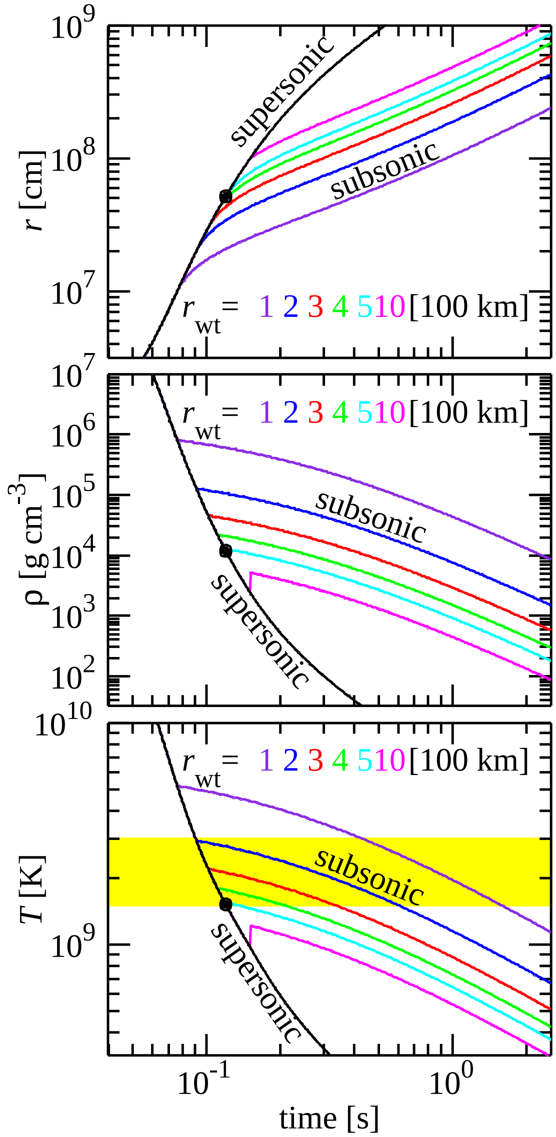

FIG. 1.— Radius (top), density (middle), and temperature (bottom) as a function of time (set to 0 at the neutrino sphere) for $M_{\rm ns} = 1.4\,M_\odot$ and $L_\nu = 1 \times 10^{52}$ erg s^{-1}. Subsonic outflows after wind termination at $r_{\rm wt} = 100, 200, 300, 400, 500$, and 1000 km are color coded. The black line shows the supersonic outflow without wind termination. In each panel, a filled circle marks the sonic point. The yellow band in the bottom panel indicates the temperature range ($T_9 = 1.5 - 3$) relevant to the νp-process.

In previous studies (Fröhlich et al. 2006a,b; Pruet et al. 2006; Wanajo 2006), some of these parameters were varied to test their sensitivities, but only for some limited cases. In particular, the effect of wind termination has not been discussed at all in previous studies. As the key nuclear reactions, we take triple-α, ^{7}Be$(\alpha,\gamma)^{11}$C, ^{10}B$(\alpha,p)^{13}$C (all relevant to the breakout from the pp-chain region), and the (n,p) reactions on ^{56}Ni, ^{60}Zn, and ^{64}Ge (§ 4). We then discuss the possible role of the νp-process as the astrophysical origin of the p-nuclei (§ 5). A summary of our results follows in § 6.

2. NEUTRINO-DRIVEN WIND MODEL AND REACTION NETWORK

The thermodynamic trajectories of neutrino-driven outflows are obtained using a semi-analytic, spherically symmetric, general relativistic model of neutrino-driven winds. This model has been developed in previous r-process (Wanajo et al. 2001; Wanajo 2007) and νp-process (Wanajo 2006) studies. Here, we describe several modifications added to the previous version.

The equation of state for ions (ideal gas) and arbitrarily degenerate, arbitrarily relativistic electrons and positrons is taken from Timmes & Swesty (2000). The root-mean-square averaged energies of neutrinos are taken to be 12, 14, and 14 MeV, for electron, anti-electron, and the other types of neutrinos, respectively, in light of a recent self-consistently exploding model of a $9M_\odot$ star (Kitaura, Janka, & Hillebrandt 2006; Hüdepohl et al. 2009; Müller, Janka, & Dimmelmeier 2010). These values are consistent with other recent studies for more massive progenitors (e.g., Fischer et al. 2009), but substantially smaller than those taken in previous works (e.g., 12, 22, and 34 MeV in Wanajo et al. 2001). The mass ejection rate $\dot{M}$ at the neutrino sphere is determined in order for the outflow to become supersonic (i.e., *wind*) through the sonic point.

The neutron star mass $M_{\rm ns}$ is taken to be $1.4\,M_\odot$ for our standard model. The radius of neutrino sphere is assumed to be $R_\nu(L_\nu) = (R_{\nu 0} - R_{\nu 1})(L_\nu/L_{\nu 0}) + R_{\nu 1}$ as a function of the neutrino luminosity L_ν (taken to be the same for all the flavors), where $R_{\nu 0} = 30$ km, $R_{\nu 1} = 10$ km, and $L_{\nu 0} = 10^{52.6} = 3.98 \times 10^{52}$ ergs s^{-1}. This roughly mimics the evolution of R_ν in recent hydrodynamic simulations (e.g., Buras et al. 2006). The wind solution is obtained with $L_\nu = 1 \times 10^{52}$ erg s^{-1} ($R_\nu = 12.5$ km) for the standard model. The time variations of radius r from the center, density ρ, and temperature T for the standard model are shown in Figure 1 (black line).

The time variations of r, ρ, and T after the wind-termination by the preceding supernova ejecta are calculated as follows. This phase is governed by the evolution of the preceding slowly outgoing ejecta, independent of the wind solution. In light of recent hydrodynamical calculations (e.g., Arcones et al. 2007), we assume the time evolution of the outgoing ejecta to be $\rho \propto t^{-2}$ and $T \propto t^{-2/3}$, where t is the post-bounce time. With these relations, we have

$$\rho(t) = \rho_{\rm wt}\left(\frac{t}{t_{\rm wt}}\right)^{-2}, \tag{1}$$

$$T(t) = T_{\rm wt}\left(\frac{t}{t_{\rm wt}}\right)^{-\frac{2}{3}}, \tag{2}$$

$$r(t) = r_{\rm wt}\left[1 - \frac{u_{\rm wt}t_{\rm wt}}{r_{\rm wt}} + \frac{u_{\rm wt}t_{\rm wt}}{r_{\rm wt}}\left(\frac{t}{t_{\rm wt}}\right)^3\right]^{\frac{1}{3}}, \tag{3}$$

$$u(t) = u_{\rm wt}\left[1 - \frac{u_{\rm wt}t_{\rm wt}}{r_{\rm wt}} + \frac{u_{\rm wt}t_{\rm wt}}{r_{\rm wt}}\left(\frac{t}{t_{\rm wt}}\right)^3\right]^{-\frac{2}{3}}\left(\frac{t}{t_{\rm wt}}\right)^2 \tag{4}$$

for $t > t_{\rm wt}$, where $t_{\rm wt}$, $u_{\rm wt}$, $r_{\rm wt}$, $\rho_{\rm wt}$, and $T_{\rm wt}$ are the time, velocity, radius, density, and temperature, respectively, just after the wind-termination. Equation (4) represents the time variation of velocity after the wind-termination. In case that $r_{\rm wt}$ is larger than that at the sonic point, $r_{\rm s}$, the Rankine-Hugoniot shock-jump conditions are applied at $r_{\rm wt}$ to obtain $u_{\rm wt}$, $\rho_{\rm wt}$, and $T_{\rm wt}$ (see, e.g., Arcones et al. 2007; Kuroda, Wanajo, & Nomoto 2008). Equations (3) and (4) are obtained from equation (1) with the steady-state condition, i.e., $r^2\rho u$ = constant (see Panov & Janka 2009). Note that equations (3) and (4) gives $r(t) \propto t$ and $u(t)$ = constant for $t \gg t_{\rm wt}$. In order to obtain t in equations (1)-(4) for a given trajectory with L_ν, the time evolution of L_ν at the neutrino sphere is assumed to be $[L_\nu(t)]_{r=R_\nu} = L_{\nu 0}(t/t_0)^{-1}$, where $t > t_0 = 0.2$ s (Wanajo 2006). With this relation, the post-bounce time is determined to be $t = (L_{\nu 0}/L_\nu)t_0 + t_{\rm loc}$, where $t_{\rm loc}$ is the local time in each wind trajectory ($t_{\rm loc} = 0$ at the neutrino sphere). The curves for various $r_{\rm wt}$ as a function of $t_{\rm loc}$ obtained from equations (1)-(3) are shown in Figure 1.

The nucleosynthetic abundances in the neutrino-driven outflows are calculated in a post-processing step by solving an extensive nuclear reaction network code. The network consists of 6300 species between the proton- and neutron-drip lines predicted by the recent fully microscopic mass formula (HFB-9, Goriely et al. 2005), all the way from single neutrons and protons up to the $Z = 110$ isotopes. All relevant reactions, i.e. (n,γ), (p,γ), (α,γ), (p,n), (α,n), (α,p), and their inverses are included (for more detail, see Wanajo et al. 2009). The rates for neutrino capture on free nucleons and ^{4}He and for neutrino spallation of free nucleons from ^{4}He (Woosley et al. 1990; McLaughlin, Fuller, & Wilson 1996) are also included. Neutrino-induced reactions of heavy nuclei are not taken into account in this study, which are expected to make only minor effects in this study.

Each nucleosynthesis calculation is initiated when the temperature decreases to $T_9 = 9$, where $T_9 \equiv T/10^9$ [K], at which only free nucleons exist. The initial compositions are then given by the electron fraction $Y_{\rm e,9}$ (proton-to-baryon ratio) at $T_9 = 9$, such as $Y_{\rm e,9}$ and $1 - Y_{\rm e,9}$ for the mass fractions of free protons and neutrons, respectively.

3. UNCERTAINTIES IN SUPERNOVA DYNAMICS

In the following subsections, we examine how the nucleosynthesis of the νp-process is influenced by varying the wind-termination radius $r_{\rm wt}$ (or temperature; § 3.1), L_ν (§ 3.2), $M_{\rm ns}$ (§ 3.3), and $Y_{\rm e,9}$ (§ 3.4) from their fiducial values 300 km (or 2.19×10^9 K), 1×10^{52} erg s^{-1}, $1.4\,M_\odot$, and 0.600, respectively, of our standard model (1st line in Table 1). All the explored models and their major outcomes are summarized in Table 1 (the first 4 columns represent the input parameters).

3.1. *Wind-termination Radius*

Recent hydrodynamic studies of core-collapse supernovae have shown that the neutrino-driven outflows develop to be supersonic, which abruptly decelerate by the reverse shock from the outer layers (e.g., Janka & Müller 1995, 1996; Burrows et al. 1995; Buras et al. 2006). Arcones et al. (2007) have explored the effects of the reverse shock on the properties of neutrino-driven winds by one-dimensional, long-term hydrodynamic simulations of core-collapse supernovae. Their result shows that, in all of their models ($10-25\,M_\odot$ progenitors), the outflows become supersonic and form the termination shock when colliding with the slower preceding supernova ejecta.

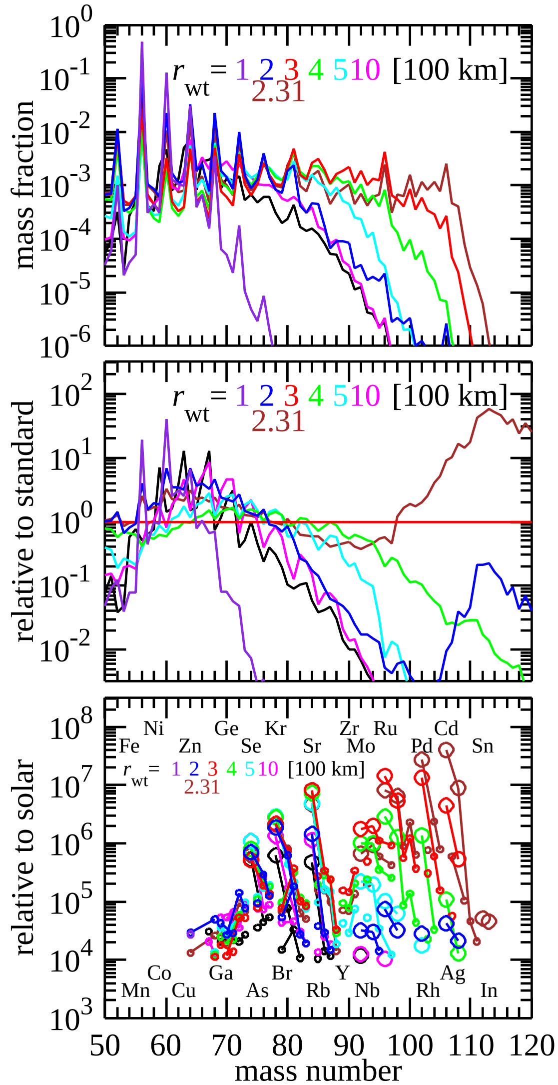

FIG. 2.— Comparison of the nucleosynthetic results for various wind-termination radii $r_{\rm wt}$. The mass fractions (top) and their ratios relative to those for the standard model (middle) are shown as a function of atomic mass number. The bottom panel shows the abundances of isotopes (connected by a line for a given element) relative to their solar values, where those lower than 10^4 are omitted. The color coding corresponds to different values of $r_{\rm wt}$ as indicated in each panel (red is the standard model). The result for the outflow without wind termination is shown in black. In the bottom panel, the names of elements are specified in the upper (even Z) and lower (odd Z) sides at their lightest mass numbers.

This condition continues until the end of their computations (10 seconds after core bounce) in their all of "standard" models with reasonable parameter choices. A recent self-consistently exploding model of a $9\,M_\odot$ star also shows qualitatively the same result (Hüdepohl et al. 2009).

In this subsection, we explore the effect of the wind-termination on the νp-process. The termination point is located at $r_{\rm wt}$ = 100, 200, 231, 300 (standard model), 400, 500, and 1000 km on the transonic wind trajectory (black line) shown in Figure 1 (top panel). The other parameters L_ν, $M_{\rm ns}$, and $Y_{\rm e,9}$ are kept to be the fiducial values (Table 1; 2nd to 9th lines). In Figure 1 (middle and bottom panels), we find shock-jumps of density and temperature by wind termination only for the $r_{\rm wt} = 1000$ km

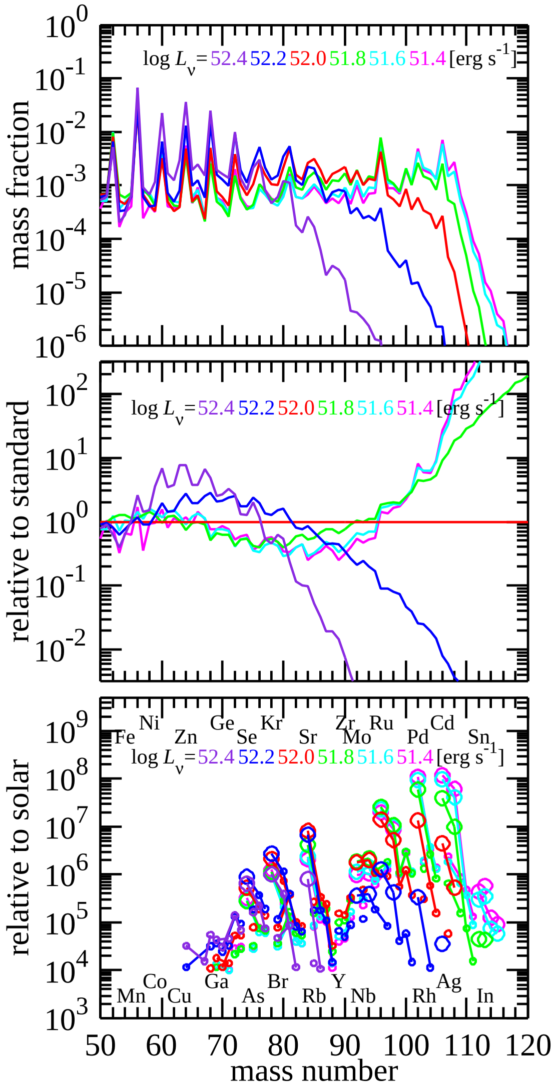

FIG. 3.— Same as Figure 2, but for various neutrino luminosities (L_ν).

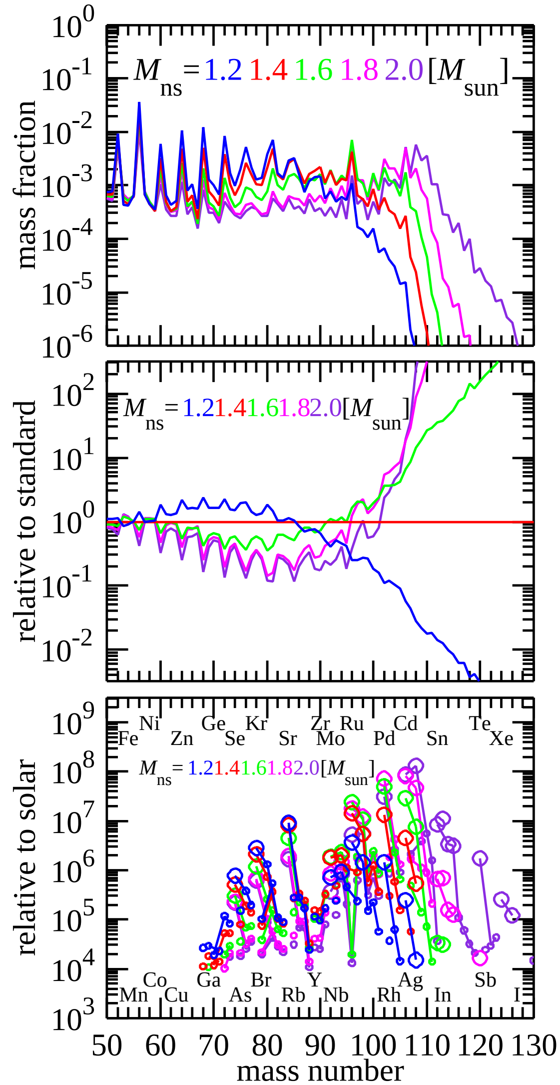

FIG. 4.— Same as Figure 2, but for various neutron star masses ($M_{\rm ns}$).

case, since the termination points are placed below the sonic radius ($r_{\rm s}$ = 515 km; Figure 1, top panel) for the other cases.[4]

The result of nucleosynthesis calculations is shown in Figure 2. The top panel shows the mass fractions, X_A, of nuclei as a function of atomic mass number, A. We find that the case with $r_{\rm wt} = 231$ km has the maximum efficiency of producing nuclei with $A = 100 - 110$ (including our calculations not shown here). The middle and bottom panels show, respectively, the mass fractions relative to the standard model ($= X_A/X_{A,\rm standard}$) and to their solar values (Lodders 2003), i.e., the overproduction factor f ($= X_i/X_{i,\odot}$ for i-th isotope), as a function of A.

[4] The outflows with $r_{\rm wt} < r_{\rm s}$ are subsonic all the way. This happens in the early wind phase when the slowly outgoing ejecta is still close to the core (Arcones et al. 2007). In this case, however, the mass ejection rate from the core is expected to be close to that of the transonic solution (with the maximum $\dot{M}$). Thus, the time variations of r, ρ, and T may not be substantially different from those of the transonic case for $r < r_{\rm wt}$ (see, e.g., Otsuki et al. 2000). We take, therefore, the transonic solution for all the cases, rather than the subsonic solution by introducing an additional free parameter $\dot{M}$.

We find a noticeable effect of wind termination on the νp-process; the production of p-nuclei between $A = 90$ and 110 is outstanding for the cases with $r_{\rm wt} = 231$ and 300 km (standard model).

It should be noted that the asymptotic entropy S ($= 57.0$ per nucleon in units of the Boltzmann constant $k_{\rm B}$; Table 1) is the same for all the cases here (except for $r_{\rm wt} = 1000$ km owing to the termination-shock heating). The reason for these different outcomes is in fact due to the different expansion timescales after wind termination. As indicated by the yellow band in Figure 1 (bottom panel), we find substantial differences in the temperature histories before or during the νp-process phase (defined as $T_9 = 1.5 - 3$, see Pruet et al. 2006; Wanajo 2006).

We define two expansion timescales τ_1 and τ_2; the former is the time elapsed from $T_9 = 6$ to $T_9 = 3$ and the latter from $T_9 = 3$ to $T_9 = 1.5$. These represent the durations of the seed production and of the νp-process, respectively. As can be seen in Figure 1 (bottom panel), τ_1 ($= 17.5$ ms) and thus the proton-to-seed ratio $Y_{\rm p}/Y_{\rm h}$ ($= 124$) at $T_9 = 3$ are the same except for the case with

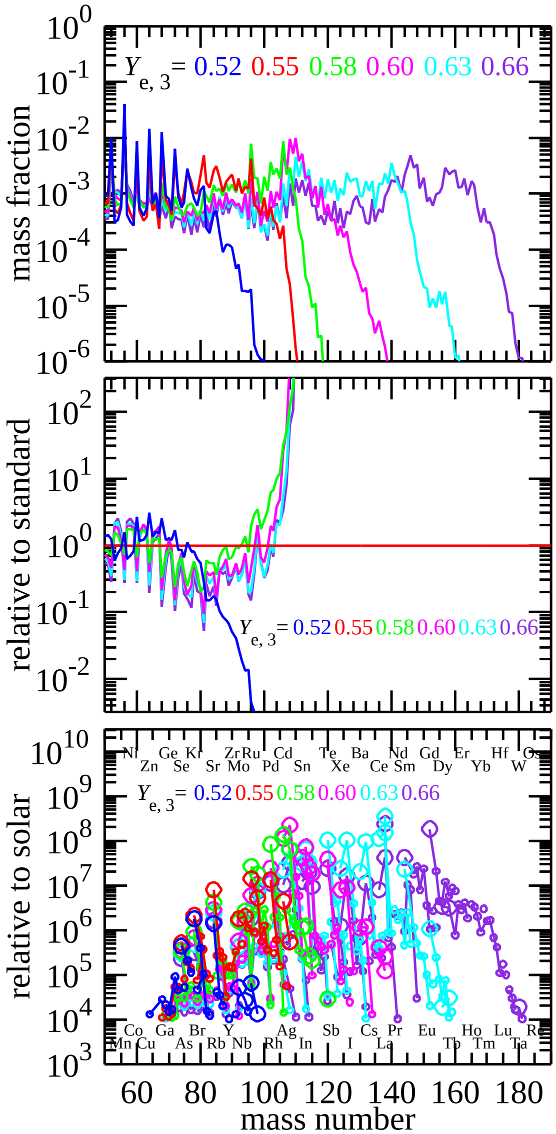

FIG. 5.— Same as Figure 2, but for various electron fractions ($Y_{e,3}$).

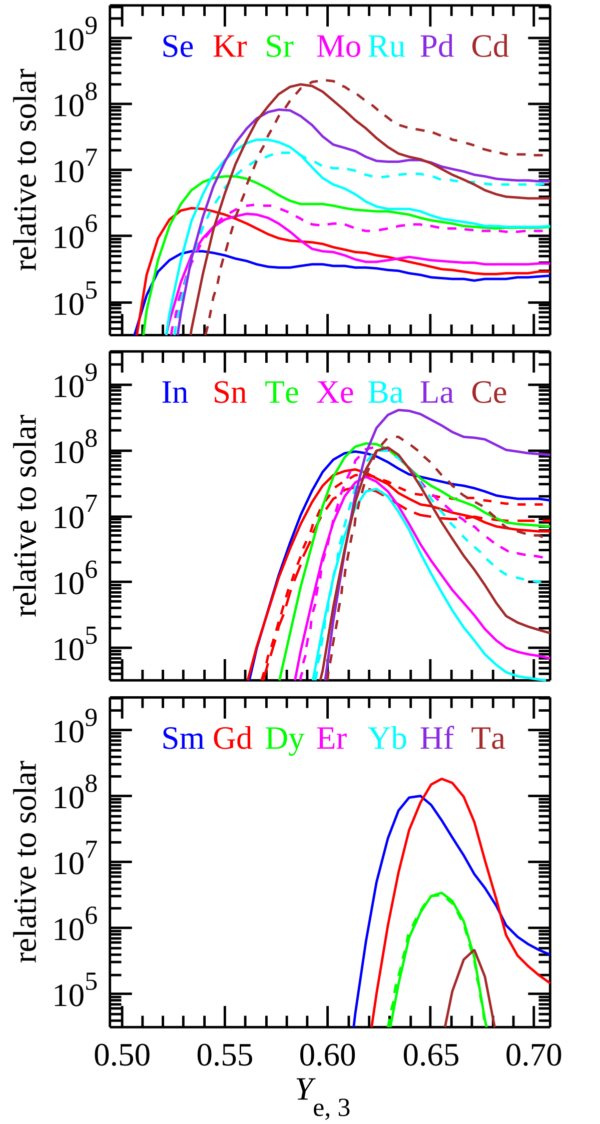

FIG. 6.— Nucleosynthetic p-abundances relative to their solar values (overproduction factors) as a function of $Y_{e,3}$. M_{ns}, L_ν, and r_{wt} are kept to be their fiducial values (1st line in Table 1). Each element is color coded with the solid, dashed, and long-dashed lines for the lightest, second-lightest, and third-lightest (^{115}Sn is only the case) isotopes, respectively (see 1st column of Table 3 for the list of p-nuclei).

$r_{wt} = 100$ km, where Y_p and Y_h are the abundances of free protons and of heavy nuclei with $Z > 2$, respectively. Nevertheless, the different values of τ_2 lead to the different efficiencies of the νp-process. We find that τ_2 of a few 100 ms (Table 1) is needed for an efficient p-nuclei production. In addition, the temperature at the wind-termination $T_{wt,9} \sim 2-3$ (in units of 10^9 K; Table 1) leads to efficient νp-processing. For the standard model ($r_{wt} = 300$ km and $T_{wt,9} = 2.19$), the maximum overproduction factor (f_{max} in Table 1) is obtained at $A = 96$ (^{96}Ru; nuc(f_{max}) in Table 1)[5]. We have the optimal overproduction ($\log f_{max} = 7.67$ at ^{106}Cd) with $T_{wt,9} = 2.65$ when the termination point is set to $r_{wt} = 231$ km (shown in Figure 2 and Table 1).

In Table 1, the nuclide with the largest mass number A_{max} with $f > f_{max}/10$ is also shown (e.g., ^{106}Cd for the standard model; nuc(A_{max}) in Table 1), which is taken to be the largest A of the p-nuclei synthesized by the νp-process. Given that our standard model represents a typical supernova condition, this implies that the νp-process can be the source of the solar p-abundances up to $A \sim 110$ (see § 5 for more detail). However, this favorable condition is not robust against a variation of r_{wt} (and thus T_{wt}); the outflows with $r_{wt} = 200$ km ($T_{wt,9} = 2.95$) and $r_{wt} \geq 500$ km ($T_{wt,9} < 1.55$) end up with $A_{max} = 84$ (^{84}Sr; Table 1). Note that the outflow with $r_{wt} = 1000$ km leads to a similar result as that without wind termination (black line in Figure 2; $r_{wt} = \infty$ in Table 1). This indicates that the role of wind termination is unimportant for $T_{wt,9} < 1.5$.

We find no substantial νp-processing for the outflow with $r_{wt} = 100$ km (Figure 2). This is due to the sub-

[5] The termination of νp-processing is due to the temperature decrease (below $T_9 \approx 1.5$), not the exhaustion of free protons (i.e., *proton-rich freezeout*). Therefore, an estimation of the maximum mass number such as $A_{max} \sim A(^{56}\mathrm{Ni}) + Y_p/Y_h = 56 + 124 = 180$ is not applicable in this case (unlike the r-process).

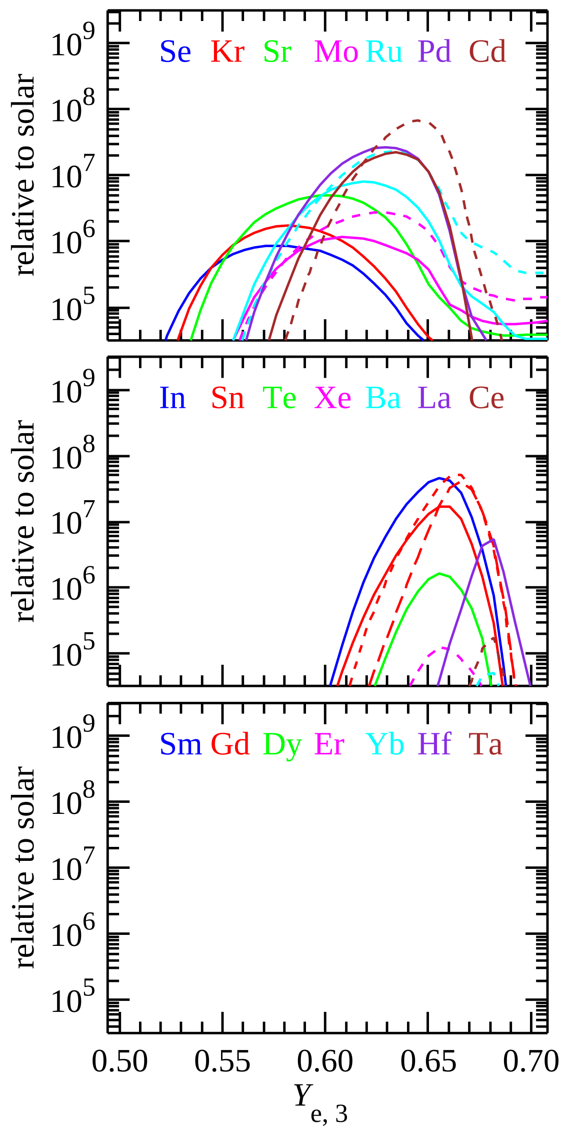

FIG. 7.— Same as Figure 6, but for the case without wind termination ($r_{\rm wt} = \infty$).

stantially smaller $Y_{\rm e}$ at the beginning of the νp-process ($T_9 = 3$), $Y_{\rm e,3} = 0.509$ (only slightly proton-rich), than those for the other cases (0.550; Table 1). As a result, $Y_{\rm p}/Y_{\rm h}$ at $T_9 = 3$ is only 1.78, which is 70 times smaller than those for the other cases. It should be noted that $Y_{\rm e,3}$ is always lower than $Y_{\rm e,9}$ (= 0.600 in the present cases). This is due to a couple of neutrino effects. One is that the asymptotic equilibrium value of $Y_{\rm e}$ in the non-degenerate matter consisting of free nucleons, which is subject to neutrino capture, is $Y_{\rm e,a} \approx 0.56$ (see, e.g., Qian & Woosley 1996) with the neutrino luminosities and energies taken in this study. Hence, the value starts relaxing from $Y_{\rm e,9}$ toward $Y_{\rm e,a}$ as soon as the calculation initiates. The other effect is due to the continuous α-particle formation ($T_9 < 7$) from interconverting free protons and free neutrons that is subject to neutrino capture, which drives $Y_{\rm e}$ towards 0.5 ("α-effect", Meyer, McLaughlin, & Fuller 1998). In the $r_{\rm wt} = 100$ km case, the wind-termination takes place at high temperature ($T_{\rm wt,9} = 5.19$) and thus the long τ_1 (= 359 ms) leads to the low $Y_{\rm e,3}$ owing to the neutrino effects.

In summary, our exploration here elucidates a crucial role of wind termination on the νp-process. On one hand, a fast expansion above the temperature $T_9 \sim 3$ (more precisely, $T_9 = 2.65$ in the present condition) is favored to obtain a high proton-to-seed ratio at the onset of the νp-process. On the other hand, a slow expansion below this temperature, owing to wind termination, is needed for efficient νp-processing. We presume that the reason for somewhat different outcomes in previous studies of the νp-process (described in § 1) is due to their different behaviors of wind termination.

3.2. *Neutrino Luminosity*

The neutrino luminosity L_ν decreases with time from its initial value of a few 10^{52} erg s^{-1} to $\sim 10^{51}$ erg s^{-1} during the first 10 s (Fischer et al. 2009; Hüdepohl et al. 2009). In this subsection, we examine the effect of L_ν on the νp-process, by varying its value from $10^{52.4} = 2.51 \times 10^{52}$ erg s^{-1} to 10 times smaller than that with an interval of 0.2 dex (from 10th to 15th lines in Table 1 and Figure 3). $M_{\rm ns}$ and $Y_{\rm e,9}$ are taken to be the fiducial values of $1.4\,M_\odot$ and 0.600, respectively. In § 3.1, we found that the temperature at the wind-termination, $T_{\rm wt}$, plays a crucial role for the νp-process. Hence, we adjust $r_{\rm wt}$ (Table 1) such that the fiducial value of $T_{\rm wt,3} = 2.19$ is obtained for each L_ν.

The results of nucleosynthesis calculations are shown in Figure 3 and Table 1. We clearly see the increasing efficiency of νp-processing with the decrease of L_ν. This is due to a larger entropy for a smaller L_ν (Table 1), while the expansion timescales τ_1 (prior to the νp-process) are similar[6]. This leads to a higher $Y_{\rm p}/Y_{\rm h}$ at the onset of the νp-process for a lower L_ν.

It should be noted that in our explored cases, $r_{\rm wt}$ decreases with decreasing L_ν (Table 1) in order to obtain the fiducial value of $T_{\rm wt,9} = 2.19$ (to figure out solely the effect of L_ν). However, if $r_{\rm wt}$ increases with time and thus $T_{\rm wt}$ decreases with decreasing L_ν, as in many explosion models, only the early stage of the neutrino-driven wind with $L_\nu \sim 10^{52}$ erg s^{-1} may be relevant to the high $T_{\rm wt,9} = 1.5 - 3$ (see, e.g., Arcones et al. 2007) that is needed for efficient νp-processing (§ 3.1).

3.3. *Neutron Star Mass*

The mass of the proto-neutron star $M_{\rm ns}$ can be somewhat different from its canonical value of $1.4\,M_\odot$, depending on its progenitor mass. In this subsection, we examine the nucleosynthesis calculations with $M_{\rm ns} = 1.2, 1.4, 1.6, 1.8$, and $2.0\,M_\odot$, while L_ν and $Y_{\rm e,9}$ are kept to be their fiducial values of 10^{52} erg s^{-1} and 0.600. For each case, the fiducial value of $T_{\rm wt,9} = 2.19$ is obtained by adjusting $r_{\rm wt}$ (from 16th to 20th lines in Table 1) as in § 3.2.

We find a clear correlation between an increase of $M_{\rm ns}$ and an increasing efficiency of νp-processing in Figure 4 and Table 1. This is due to a larger S and a smaller τ_1

[6] When the radius of the neutrino sphere R_ν is fixed to a constant value, the expansion timescale increases with decreasing L_ν(see, e.g. Otsuki et al. 2000; Wanajo et al. 2001). In this study, however, R_ν is assumed to decrease with decreasing L_ν (§ 2), which is more realistic. As a result, the difference of τ_1 in the range of L_ν explored here is moderate.

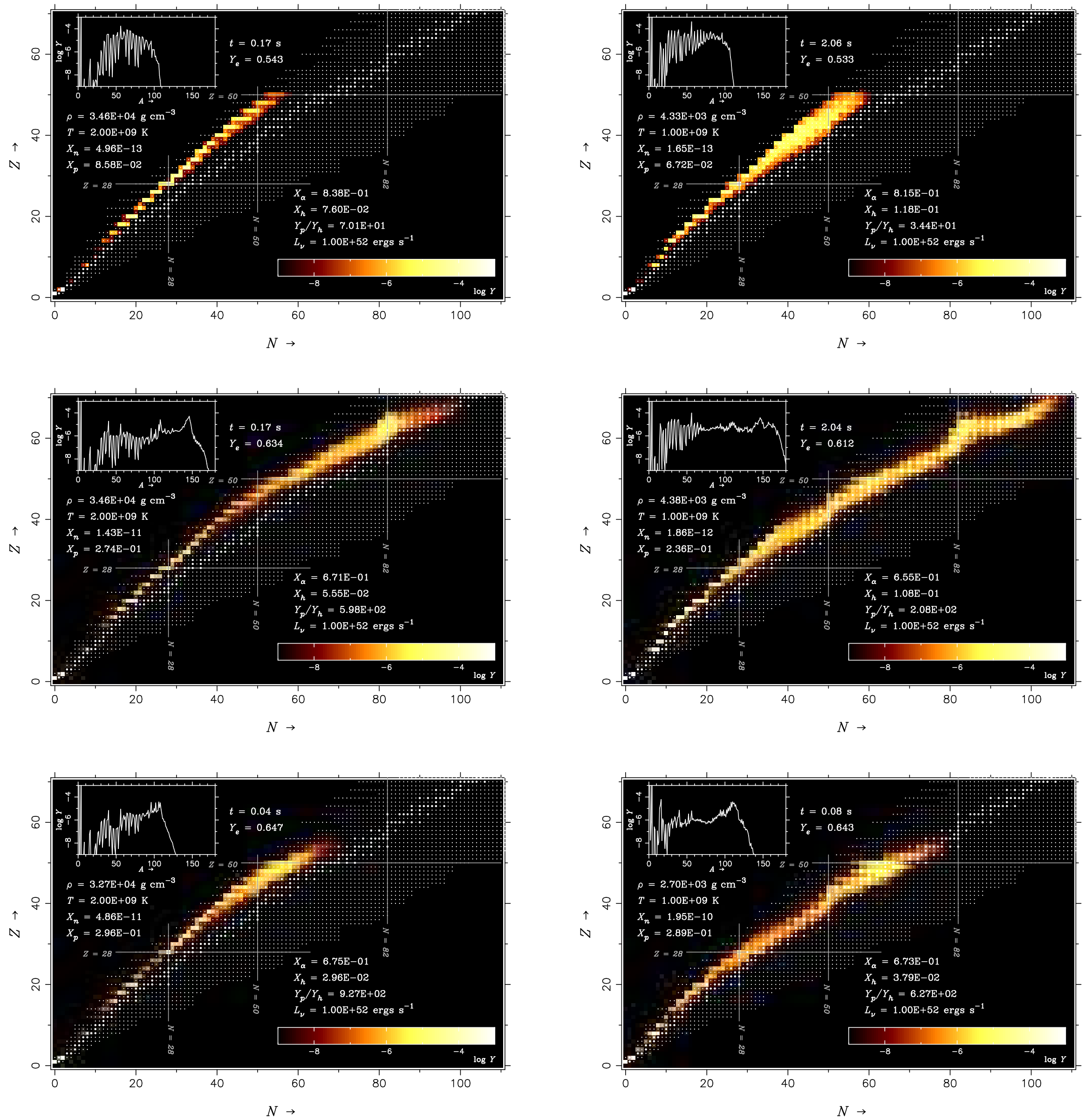

FIG. 8.— Snapshots of nucleosynthesis on the nuclear chart when the temperature drops to $T_9 = 2$ (left) and 1 (right). Top, middle, and the bottom panels are for the standard model (1st line in Table 1), that with $Y_{\mathrm{e},9}$ replaced by 0.800 ($Y_{\mathrm{e},3} = 0.655$), and that with $Y_{\mathrm{e},9}$ and r_{wt} replaced by 0.800 and ∞ (without wind termination). The nucleosynthetic abundances are color coded. The species included in the reaction network are shown by dots (with the thick dots for the stable isotopes). The abundance distribution as a function of atomic mass number is shown in the inset of each panel.

for a larger M_{ns} (e.g., Otsuki et al. 2000; Wanajo et al. 2001), both of which help to increase $Y_{\mathrm{p}}/Y_{\mathrm{h}}$. This implies that a more massive progenitor (up to $\sim 30\,M_\odot$) that forms a neutron star is favored for the νp-process. It should be emphasized, however, that the outflow with a typical mass of $M_{\mathrm{ns}} = 1.4\,M_\odot$ can provide the sufficient physical conditions for producing the p-nuclei up to $A \sim 110$.

3.4. *Electron Fraction*

The electron fraction Y_{e} is obviously one of the most important ingredients in the νp-process as it controls the proton-richness in the ejecta. Recent hydrodynamical studies with elaborate neutrino transport indicate that Y_{e} exceeds 0.5 and increases up to ~ 0.6 during the neutrino-driven wind phase (Fischer et al. 2009; Hüdepohl et al. 2009). It should be noted that Y_{e} substantially decreases from its initial value owing to the neutrino effects (§ 3.1). In our standard model, the value decreases from $Y_{\mathrm{e},9} = 0.600$ (at $T_9 = 9$) to $Y_{\mathrm{e},3} = 0.550$ at the onset of the νp-process ($T_9 = 3$). However, these neutrino effects would highly dependent on the neutrino luminosities and energies of electron and anti-electron neutrinos assumed in this study. In this subsection, therefore, we take the value at the onset of the νp-process, $Y_{\mathrm{e},3}$, as a reference, rather than the initial value $Y_{\mathrm{e},9}$.

Figure 5 and Table 1 (the last 6 lines) show the nucleosynthetic results for $Y_{\mathrm{e},3} = 0.523, 0.550, 0.576, 0.603, 0.629,$ and 0.655 (see Table 1 for their initial values $Y_{\mathrm{e},9}$). The other parameters M_{ns}, L_ν, and r_{wt} (and thus T_{wt}) are kept to be their fiducial values (1st line in Table 1). We find a great im-

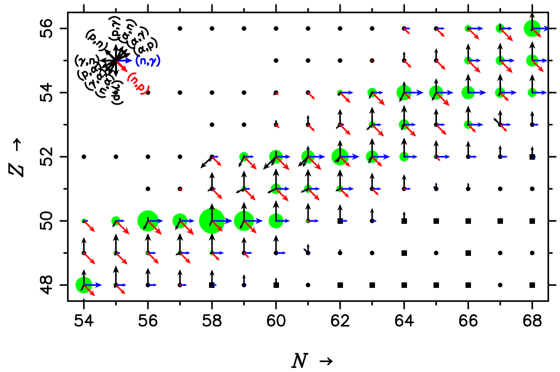

FIG. 9.— Nuclear flows (arrows) and the abundances (circles) near the end point of the classical *rp*-process ($Z = 52$) in logarithmic scale for the model with $Y_{\rm e,3} = 0.655$ (last line in Table 1) when the temperature decreases to $T_9 = 2$ (that corresponds to the middle-left panel in Figure 8). The nuclei included in the reaction network are denoted by dots, with the stable isotopes represented by squares. The flows by β^+-decays (not shown here) are negligible compared to those by (n,p) reactions (red arrows). Radiative neutron capture (blue arrows) also plays a significant role.

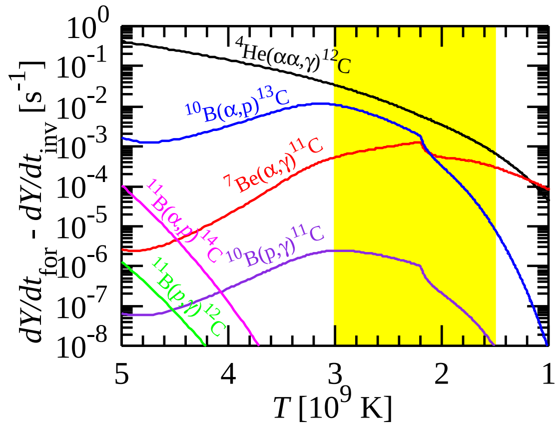

FIG. 10.— Nuclear flows for the reactions that bridge from $Z < 6$ (the *pp*-chain region) to $Z = 6$ as a function of temperature. The nuclear flow is defined as the deference of the time-derivatives (per second) of abundance between the forward and inverse reactions for a given channel. The yellow band indicates the temperature range relevant to the νp-process ($T_9 = 1.5 - 3$).

pact of the $Y_{\rm e}$ variation; an increase of only $\Delta Y_{\rm e,3} \sim 0.03$ leads to a 10-unit increase of $A_{\rm max}$, while $f_{\rm max}$ is similar for $Y_{\rm e,3} > 0.550$.

In order to elucidate the effect of $Y_{\rm e}$ in more detail, the overproduction factor f for each *p*-nucleus is drawn in Figure 6 as a function of $Y_{\rm e,3}$, where $M_{\rm ns}$, L_ν, and $r_{\rm wt}$ are kept to be their fiducial values. Each element is color coded with the solid, dashed, and long-dashed lines for the lightest, second-lightest, and third-lightest (^{115}Sn is only the case) isotopes, respectively (see 1st column of Table 3 for the list of *p*-nuclei). We find in the top panel of Figure 6 that the *p*-nuclei up to $A = 108$ (^{108}Cd) take the maximum overproduction factors between $Y_{\rm e,3} = 0.53$ and 0.60. Given the maximum $Y_{\rm e,3}$ to be ~ 0.6 according to some recent hydrodynamic results (e.g., Fischer et al. 2009; Hüdepohl et al. 2009), this implies that the maximum mass number of the *p*-nuclei produced by the νp-process is $A \sim 110$.

In principle, the heavier *p*-nuclei can be synthesized if the matter is more proton-rich than $Y_{\rm e,3} = 0.6$. The middle panel of Figure 6 shows that the overproduction factors of the *p*-nuclei from $A = 113$ (^{113}In) up to $A = 138$ (^{138}Ce) are maximal between $Y_{\rm e,3} = 0.61$ and 0.63. Furthermore, ^{144}Sm and ^{152}Gd reach the maximum overproduction factors at $Y_{\rm e,3} = 0.64$ and 0.66, respectively (bottom panel in Figure 6). The end point of the νp-process appears to be at $A \sim 180$ (^{180}Ta) in our explored cases. It should be noted that the wind-termination plays a crucial role as well (§ 3.1). This is evident if we compare Figures 6 and 7, where the latter is the result for $r_{\rm wt} = \infty$. Without wind termination, more proton-richness ($\Delta Y_{\rm e,3} \sim 0.05$) is required for a given *p*-nucleus to be produced, but with a substantially smaller overproduction factor. The *p*-nuclei heavier than $A = 140$ cannot be produced at all without wind termination (bottom panel in Figure 7).

We can understand the reason for the above result from Figure 8, which displays the snapshots of nucleosynthesis for selected cases on the nuclear chart when the temperature drops to $T_9 = 2$ (left) and 1 (right). Top, middle, and bottom panels are for the standard model, that with $Y_{\rm e,9}$ replaced by 0.800 ($Y_{\rm e,3} = 0.655$), and that with $Y_{\rm e,9}$ and $r_{\rm wt}$ replaced by 0.800 and ∞ (without wind termination), respectively. In the standard model ($Y_{\rm e,3} = 0.550$), the nuclear flow proceeds along the proton-drip line and encounters the proton-magic number $Z = 50$ ($A \sim 100 - 110$). There are α-unbound nuclei of $^{106-108}$Te ($Z = 52$) just above $Z = 50$ along the proton-drip line, which is the end point of the classical *rp*-process (Schatz et al. 2001). This is why the νp-process stops at $A \sim 110$ for $Y_{\rm e,3} \lesssim 0.6$.

As $Y_{\rm e,3}$ exceeds 0.6, radiative neutron capture becomes more important and competes with proton capture (Pruet et al. 2006; Wanajo 2006). This is due to the large amount of free protons ($Y_{\rm p}/Y_{\rm h} = 1130$ at $T_9 = 3$ for the middle panels of Figure 8; the last line in Table 1) that release free neutrons owing to neutrino capture. As a result, the nuclear flow deviates from the end point of the classical *rp*-process ($N = 54 - 56$) at $Z = 52$ and extends to the larger atomic number through the nuclei with $N > 60$, as can be seen in Figure 9. The stagnation of the flow at the neutron-magic number $N = 82$ in the middle panels of Figure 8 clearly shows the importance of neutron capture. The concentration of nuclei at $N = 82$ leads to the large overproduction factors of the *p*-nuclei with $A = 130 - 150$ as seen in Figure 6. Note that the *p*-nuclide ^{144}Sm is located on the $N = 82$ line.

Beyond $N = 82$, the increasing atomic number and the decreasing temperature inhibit further proton capture. As a result, the nuclear flow approaches the β-stability line and finally enters to the neutron-rich region at $A \sim 160$ as seen in the middle-right panel of Figure 8. Without wind termination (but with the same parameters otherwise), however, the rapidly decreasing temperature does not allow the nuclear flow to reach $N = 82$ as seen in the bottom panels of Figure 8. This is the reason for the inefficiency of producing heavy *p*-nuclei in Figure 7.

4. UNCERTAINTIES IN NUCLEAR REACTION RATES

There have been continuing experimental works relevant to the νp-process (e.g., Weber et al. 2008) since its discovery. However, we still rely upon theoretical or old experimental estimates for the vast majority of nuclear reactions accompanied with the νp-process, which may

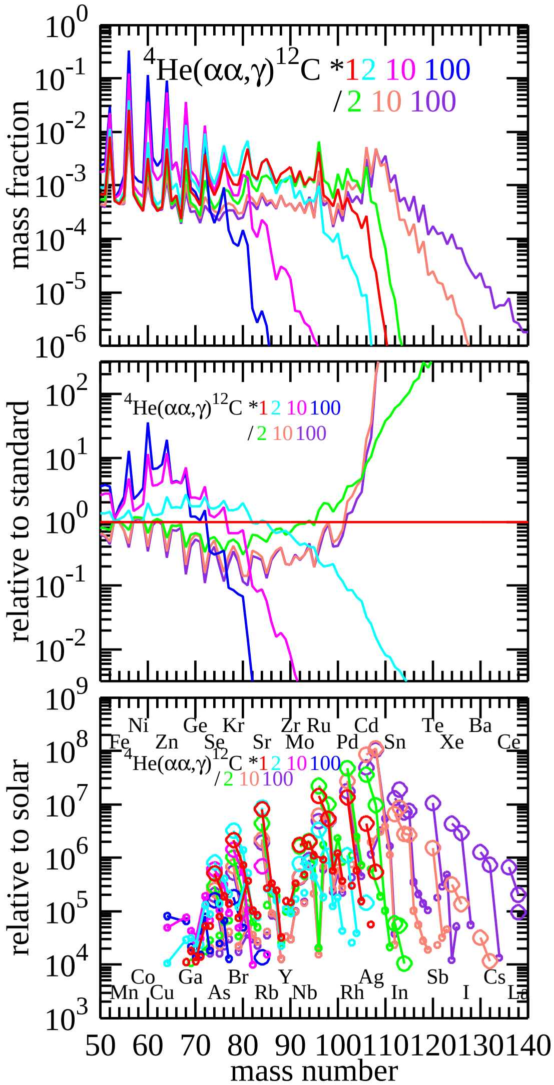

FIG. 11.— Same as Figure 2, but for variations on the triple-α reaction.

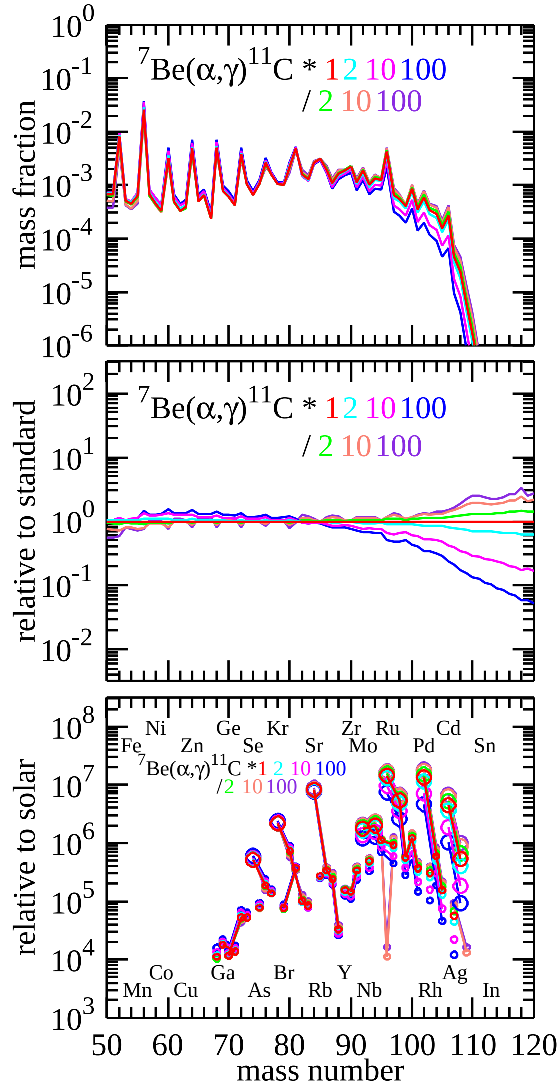

FIG. 12.— Same as Figure 2, but for variations on the $^7\mathrm{Be}(\alpha,\gamma)^{11}\mathrm{C}$ reaction.

suffer from large uncertainties. The νp-process is unique in a couple of aspects, different from the classical rp-process. First is that the seed nuclei are directly formed from free nucleons (i.e., the primary process), while the classical rp-process needs CNO seeds. Thus, the triple-α and some 2-body reactions relevant to the breakout from the pp-chain region ($Z < 6$) play important roles for setting the proton-to-seed ratio $Y_\mathrm{p}/Y_\mathrm{h}$ at the beginning of the νp-process (§ 4.1). Second is the role of neutron capture, in particular of (n,p) reactions on heavy nuclei in the proton-rich matter, which bypass the β^+-waiting points on the classical rp-process path (§ 4.2). In the following subsections, we test the effect of uncertainties in some selected reactions by simply multiplying or dividing their original values by factors of 2, 10, and 100 with the standard model (1st lines in Tables 1 and 2). All the explored results are listed in Table 2.

4.1. *Breakout from the pp-Chain Region*

In Figure 10, the nuclear flows for the reactions that bridge from $Z < 6$ (the pp-chain region) to $Z = 6$ (the CNO region) are shown as a function of the temperature before ($T_9 > 3$) and after ($T_9 < 3$) the onset of the νp-process. Here, the nuclear flow is defined as the difference between the time-derivatives of abundances for the forward and inverse reactions of a given channel. It is clear that the triple-α reaction plays a dominant role for the breakout from the pp-chain region. We find, however, a couple of 2-body reactions $^7\mathrm{Be}(\alpha,\gamma)^{11}\mathrm{C}$ and $^{10}\mathrm{B}(\alpha,p)^{13}\mathrm{C}$ compete with the triple-α reaction during the νp-process phase[7]. Therefore, we select these three reactions for the sensitivity tests. Note that the unstable isotope ^{11}C produced is followed by $^{11}\mathrm{C}(\alpha,p)^{14}\mathrm{N}$ before decaying back to ^{11}B. All the data of the above reactions are based on experiments but from old sources by Caughlan & Fowler (1988, for the first two) and Wagoner (1969, for the last) in the REACLIB[8] compilation.

The result for the triple-α reaction is shown in Fig-

[7] ^{10}B in the last reaction originates from the endothermic reaction $^7\mathrm{Be}(\alpha,p)^{10}\mathrm{B}$. Because of its small (negative) Q-value of -1.146 MeV and the larger abundance of α particles than that of protons, this reaction is slightly faster than its inverse (exothermic reaction) in the present case.

[8] http://nucastro.org/reaclib.html.

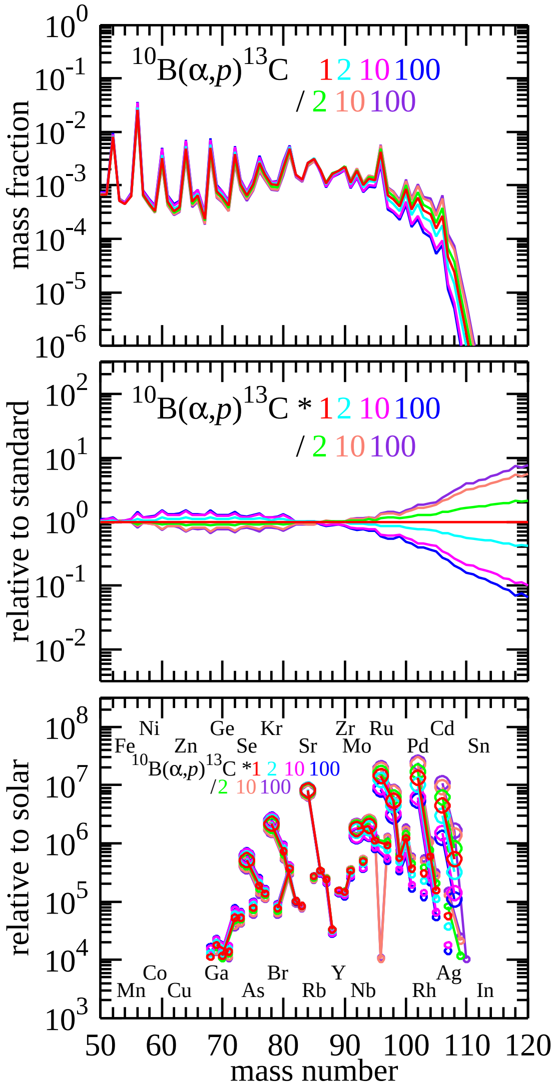

FIG. 13.— Same as Figure 2, but for variations on the $^{10}\mathrm{B}(\alpha, p)^{13}\mathrm{C}$ reaction.

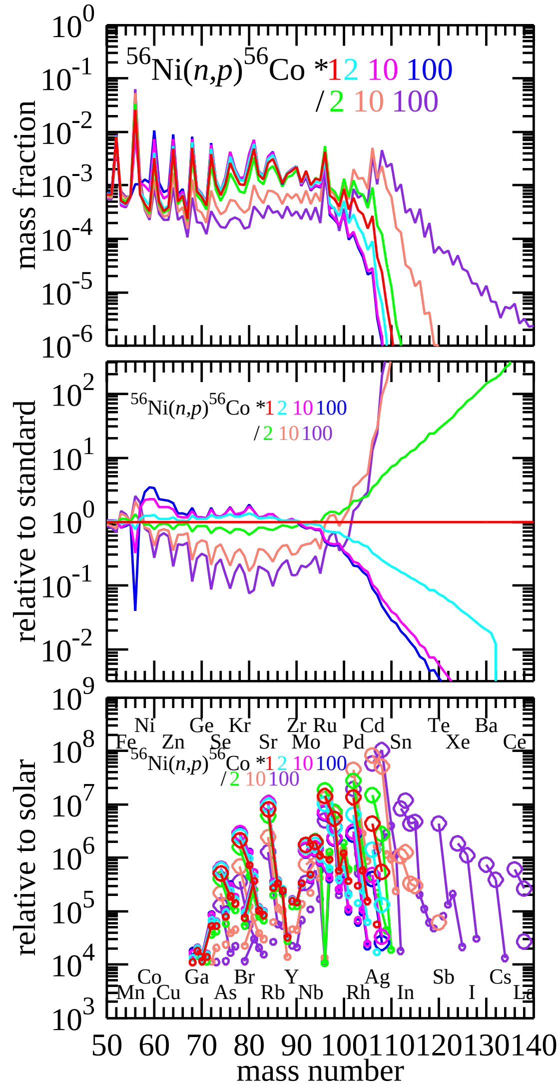

FIG. 14.— Same as Figure 2, but for variations on the $^{56}\mathrm{Ni}(n, p)^{56}\mathrm{Co}$ reaction.

ure 11, where the forward and inverse rates are multiplied or divided by factors of 2, 10, and 100. We find substantial changes in the production of p-nuclei with $A \sim 100-110$ for a factor of 2 variation on the rate, and more drastic changes for a factor of 10 (or 100) variation. The reason can be mainly attributed to the resulting proton-to-seed ratio $Y_\mathrm{p}/Y_\mathrm{h}$ (at $T_9 = 3$; Table 2). A larger triple-α rate leads to a more efficient seed production and thus a smaller $Y_\mathrm{p}/Y_\mathrm{h}$. A larger rate during the νp-process phase ($T_9 = 1.5 - 3$) also yields more carbon and other intermediate-mass nuclei that act as *proton poison*. As a result, efficiency of the νp-process decreases. The same interpretation is applicable to the opposite case with a smaller rate.

Figure 12 shows the result for $^7\mathrm{Be}(\alpha, \gamma)^{11}\mathrm{C}$. We find non-negligible differences in the p-abundances with $A \sim 100-110$, although the impact is much smaller than that for triple-α. Note that a larger rate has a more impact than the smaller rate with the same factor as can be seen in the middle panel of Figure 12. This is a consequence that the rate competes with triple-α only during the late phase of the νp-process ($T_9 \lesssim 2$; Figure 10). A larger rate during this pahse leads to more production of intermediate-mass nuclei that act as proton poison. However, a variation of this rate does not substantially affect $Y_\mathrm{p}/Y_\mathrm{h}$ at the onset of νp-processing ($T_9 = 3$; Table 2).

The result for $^{10}\mathrm{B}(\alpha, p)^{13}\mathrm{C}$ is shown in Figure 13. We find a similar level of abundance changes to that for $^7\mathrm{Be}(\alpha, \gamma)^{11}\mathrm{C}$, but also for lower rates as seen in the middle panel of Figure 13. This is because the rate competes with triple-α during the early phase of νp-process ($T_9 \sim 3$; Figure 10). Hence, a variation on the rate also affects $Y_\mathrm{p}/Y_\mathrm{h}$ at the beginning of νp-processing (Table 2).

4.2. (n, p) *Reactions on Heavy Nuclei*

The νp-process initiates at $T_9 \sim 3$ with the seed nuclei ^{56}Ni that is formed from free nucleons prior to this stage, where the (n, p) reactions mainly control the progress of nuclear flow. Currently, there are no experiment-based estimates for the (n, p) reactions on proton-rich isotopes. We therefore expect non-negligible uncertainties in the currently available Hauser-Feshbach rates for these reactions. We here pick up three (n, p) reactions starting

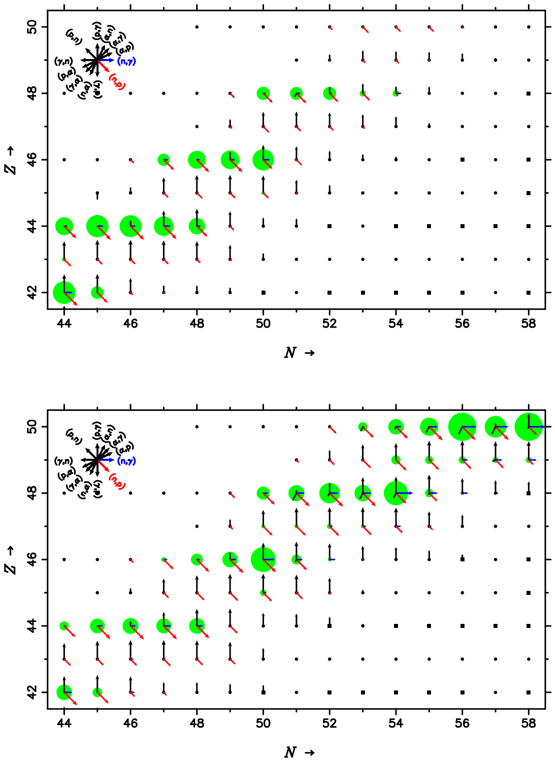

FIG. 15.— Same as Figure 9, but for the standard model (top) and that with the ^{56}Ni$(n,p)^{56}$Co rate and its inverse reduced by a factor of 100 (bottom).

from the seed nuclei along the νp-process path, i.e., on ^{56}Ni, ^{60}Zn, and ^{64}Ge. The last one, ^{64}Ge, is the first β^+-waiting point nucleus encountered in the classical rp-process path. Note that the variations on these rates do not affect $Y_{\rm p}/Y_{\rm h}$ at the onset of the νp-process (Table 2). All the data for these rates are from theoretical estimates in BRUSLIB[9] (Aikawa et al. 2005) making use of experimental masses (Audi, Wapstra, & Thibault 2003).

We find a remarkable change in the p-abundances with $A \sim 110$ by a factor of 10 with only a factor of 2 variation on ^{56}Ni$(n,p)^{56}$Co (Figure 14 and Table 2). This demonstrates that the (n,p) reaction on the first (n,p)-*waiting nucleus* ^{56}Ni plays a key role for the progress of nuclear flow. It should be noted that a smaller rate results in a larger $f_{\rm max}$ and $A_{\rm max}$ as can be seen in the bottom panel of Figure 14 and in Table 2. As shown in Figure 15, the nuclear flow stagnates at ^{96}Pd ($N = 50$ and $Z = 46$) before reaching $Z = 50$, because of the shell-closure for neutrons.[10] As a result, ^{96}Pd plays a role of the "seed" nucleus for producing nuclei heavier than $A = 96$. For the standard model, free protons and neutrons are also consumed by the nuclei lighter than $A = 96$ with similar abundances (Figure 15; top panel, also Figure 14; top panel), which are continuously supplied by the flow starting from ^{56}Ni. In contrast, the reduced ^{56}Ni$(n,p)^{56}$Co rate leads to the smaller abundances of nuclei between $A = 56$ and 96. Therefore, a larger number of free protons and neutrons are available for the "seed" nuclei ^{96}Pd (Figure 15; bottom panel, also Figure 14; top panel).

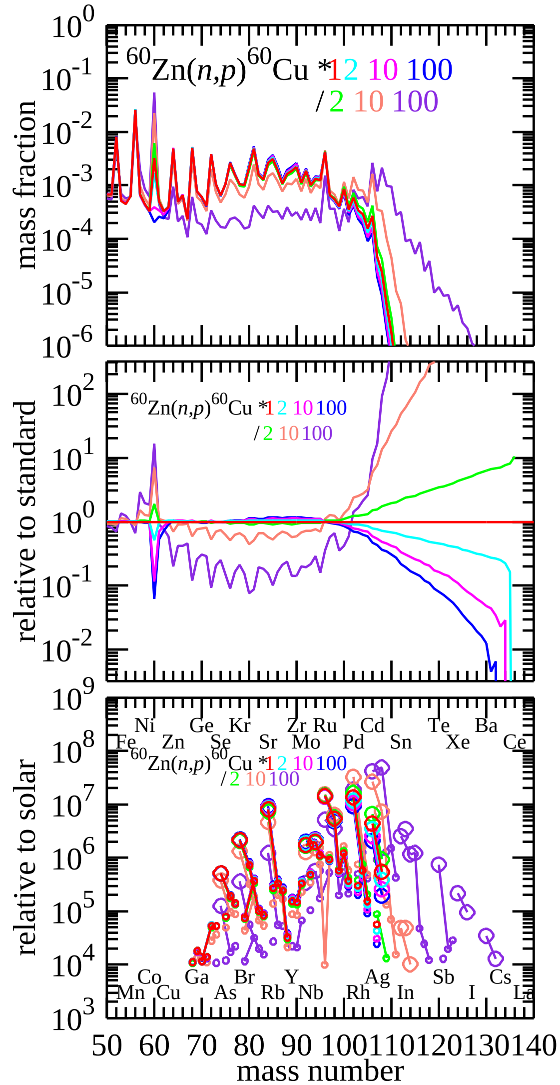

FIG. 16.— Same as Figure 2, but for variations on the ^{60}Zn$(n,p)^{60}$Cu reaction.

Figure 16 shows that the variations on the second (n,p)-waiting nucleus ^{60}Zn also lead to large (but less prominent) changes in the nucleosynthetic p-abundances. Unlike these two reactions, only the lower (n,p) rates on ^{64}Ge (the first β^+-waiting nucleus on the classical rp-process) lead to substantial changes in the nucleosynthesis of p-abundances (Figure 17). This indicates that the nuclear flow has been already regulated by the preceding (n,p)-waiting nuclei ^{56}Ni and ^{60}Zn, and only a reduced rate of ^{64}Ge$(n,p)^{64}$Ga can substantially change the p-nuclei production.

5. νp-PROCESS AS THE ORIGIN OF p-NUCLEI

In the previous sections (§ 3 and 4), we find that both the uncertainties in the supernova dynamics and nuclear reactions substantially affect the nucleosynthetic p-abundances. It is not easy, therefore, to determine the role of the νp-process as the source of the solar p-nuclei.

[9] http://www.astro.ulb.ac.be/Html/bruslib.html.

[10] Weber et al. (2008) reported the suppression of the flow through ^{87}Mo$(p,\gamma)^{88}$Tc that is clearly seen in Figure 15, when using their result of high-precision nuclear mass measurements. They showed, however, the nucleosynthetic abundances of p-nuclei were almost unchanged by this modification compared to those using the masses in Audi, Wapstra, & Thibault (2003).

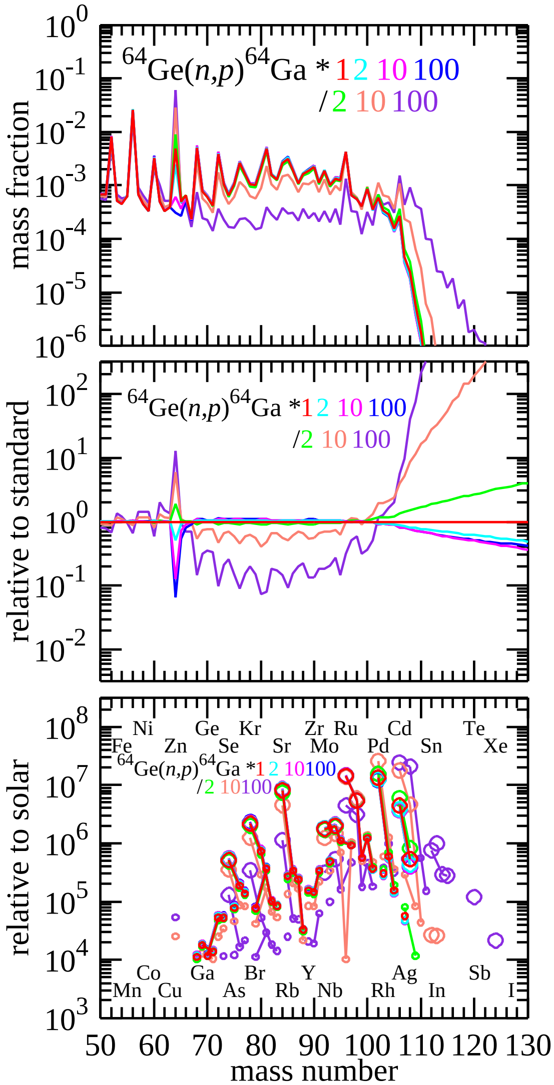

FIG. 17.— Same as Figure 2, but for variations on the ^{64}Ge$(n,p)^{64}$Ga reaction.

Keeping such uncertainties in mind, we discuss a possible contribution of the νp-process to the solar p-abundances based on our result by comparing with other possible sources.

Table 3 lists the currently proposed astrophysical origins for each p-nuclide (1st column) with its solar abundance (2nd column, Lodders 2003). All these sources are associated with core-collapse supernovae. Photodissociation of pre-existing s-process abundances in the shocked oxygen-neon layer of a core-collapse supernova, i.e., the γ-process (e.g., Prantzos et al. 1990; Rayet et al. 1995; Hayakawa et al. 2008) is currently regarded as the most successful scenario. In the 3rd column of Table 3, the p-nuclei whose origins can be explained by the γ-process in Rayet et al. (1995) are specified by "yes". The origins of 24 out of 35 p-isotopes can be explained by the γ-process. However, the light p-isotopes (^{92,94}Mo, ^{96,98}Ru, ^{102}Pd, ^{106,108}Cd, ^{113}In, and ^{115}Sn), which account for a large fraction in the solar p-abundances, and the two heavy p-isotopes (^{138}La and ^{152}Gd) need other sources (specified by "no" in Table 3).

The ν-process (4th column in Table 3, Woosley et al. 1990) in core-collapse supernovae is suggested to account for the production of a couple of heavy p-isotopes ^{138}La and ^{180}Ta (the former cannot be produced by the γ-process). The α-process (followed by successive proton capture) in slightly neutron-rich ($Y_{\rm e} \approx 0.47-0.49$) neutrino-driven outflows was also proposed as the production site of some light p-nuclei (Hoffman et al. 1996; Wanajo 2006; Wanajo et al. 2009). A recent study of nucleosynthesis in the electron-capture supernovae of a $9\,M_\odot$ star shows that the lightest p-nuclei ^{74}Se, ^{78}Kr, ^{84}Sr, and ^{92}Mo can be produced enough to account for their solar amounts (5th column in Table 3, Wanajo et al. 2009). However, these additional sources still cannot fill the gap for some light p-isotopes ^{94}Mo, ^{96,98}Ru, ^{102}Pd, ^{106,108}Cd, ^{113}In, ^{115}Sn, and for a heavy p-isotope ^{152}Gd.

Our result in this study is based on a semi-analytic model of neutrino-driven winds, while the results for the γ-process, the ν-process, and the α-process listed in Table 3 are all based on realistic hydrodynamic studies. Nevertheless, we attempt to present a list of the p-isotopes whose origin can be attributed to the νp-process, as follows. The requisite overproduction factor for a given nuclide *per supernova event*, which explains its solar origin, is inferred to be > 10 (e.g., Woosley et al. 1994). Assuming the masses of the total ejecta and of the neutrino-driven ejecta to be $\sim 10\,M_\odot$ and $\sim 10^{-3}\,M_\odot$ (e.g., Wanajo 2006), the overproduction factor per supernova event is diluted by about 4 orders of magnitude compared to our result. We thus apply the condition $f > 10^5$ and $f > f_{\rm max}/10$ to each p-isotope abundance in Figure 6 (the standard model with $Y_{\rm e,3}$ ranging between 0.5 and 0.7).

The p-isotopes that satisfy the above condition are listed in the last column of Table 3. According to recent hydrodynamic studies (Fischer et al. 2009; Hüdepohl et al. 2009), the maximum $Y_{\rm e}$ in the neutrino-driven outflows is ~ 0.6. Therefore, the p-isotopes that satisfy the above condition only with $Y_{\rm e,3} > 0.6$ are indicated by "[yes]". This implies that the νp-process in core-collapse supernovae is the possible astrophysical origin of the light p-nuclei up to $A = 108$. In principle, however, the νp-process can account for the origin of the heavy p-isotopes up to $A = 152$ as well, if $Y_{\rm e,3} \approx 0.65$ (Figure 6) is achieved in the neutrino-driven outflows. If this is true, a reasonable combination of the astrophysical sources considered here can explain all the origins of the solar p-isotopes. It should be noted that most of the maximum overproduction factors of these heavy p-nuclei are $\gtrsim 10^8$. This is three orders of magnitude larger than the above requisite value ($f = 10^5$). Thus, only $\sim 0.1\%$ of neutrino-driven ejecta with $Y_{\rm e,3} \approx 0.60-0.65$ is enough to account for the origin of these heavy p-nuclei. Future multi-dimensional hydrodynamic studies of core-collapse supernovae with full neutrino transport will be of particular importance if such a condition is indeed obtained.

6. SUMMARY

We investigated the effects of uncertainties in supernova dynamics as well as in nuclear reactions on the νp-process in the neutrino-driven outflows of core-collapse supernovae. The former includes the wind-termination radius $r_{\rm wt}$ (or temperature $T_{\rm wt}$), neutrino luminosity L_ν, neutron-star mass $M_{\rm ns}$, and electron fraction $Y_{\rm e,9}$ (or

$Y_{e,3}$, at $T_9 = 9$ and 3, respectively), while the latter the reactions relevant to the breakout from the pp-chain region ($Z < 6$) and of (n, p) on heavy nuclei ($Z \geq 56$). Our result is summarized as follows.

1. Wind termination of the neutrino-driven outflow by colliding with the preceding supernova ejecta causes a slowdown of the temperature decrease and thus plays a crucial role on the νp-process. The termination within the temperature range of $T_9 = 1.5-3$ (relevant to the νp-process) substantially enhances efficiency of the p-nuclei production (i.e., with a larger maximum mass number $A_{\rm max}$ and larger maximum overproduction factor $f_{\rm max}$). In the current case, the efficiency is maximal at $T_{\rm wt,9} = 2.65$ ($r_{\rm wt} = 231$ km). This implies that the early wind phase with the termination radius of $\sim 200 - 500$ km is favored for the νp-process.

2. A lower L_ν (with the other parameters $T_{\rm wt}$, $M_{\rm ns}$, and $Y_{e,9}$ unchanged) leads to more efficient νp-processing with larger $A_{\rm max}$ and $f_{\rm max}$. This is due to the larger entropy per nucleon for a lower L_ν, which increases the proton-to-seed ratio $Y_{\rm p}/Y_{\rm h}$ at the onset of νp-processing ($T_9 = 3$). However, the role of the wind-termination is more efficient and thus we presume that the maximum efficiency is obtained during the early phase with $L_\nu \sim 10^{52}$ erg s^{-1}.

3. A larger $M_{\rm ns}$ (with the other parameters $T_{\rm wt}$, L_ν, and $Y_{e,9}$ unchanged) results in a larger $A_{\rm max}$ and $f_{\rm max}$. This is a consequence of the larger entropy per nucleon and the faster expansion of the neutrino-driven outflow for a larger $M_{\rm ns}$, both of which help to increase $Y_{\rm p}/Y_{\rm h}$ at the onset of the νp-process. This result suggests that a more massive progenitor is favored for more efficient νp-processing.

4. The νp-process is highly sensitive to the electron fraction $Y_{e,3}$ that controls $Y_{\rm p}/Y_{\rm h}$ at the onset of the νp-process. An increase of only $\Delta Y_{e,3} \sim 0.03$ results in $\Delta A_{\rm max} \sim 10$. The models with $Y_{e,3} = 0.5-0.6$ (with the other parameters unchanged) produce sufficient amounts of the light p-nuclei up to $A = 108$. Furthermore, the models with $Y_{e,3} = 0.60 - 0.65$ produce the p-nuclei up to $A = 152$. Note that this is a combined effect of the high $Y_{e,3}$ and the wind-termination at sufficiently high temperature ($T_{\rm wt,9} = 2.19$ in the standard model). Our result shows no substantial enhancement of the p-nuclei with $A > 152$, since the nuclear flow reaches the β-stability line and enters to the neutron-rich region at $A \sim 130 - 160$.

5. Variations on the nuclear reactions relevant to the breakout from the pp-chain region ($Z < 6$), namely of triple-α, ^{7}Be$(\alpha,\gamma)^{11}$C, and ^{10}B$(\alpha,p)^{13}$C affect the νp-process by changing $Y_{\rm p}/Y_{\rm h}$ or producing intermediate-mass nuclei (proton poison) during νp-processing. Among these reactions, triple-α has the largest impact, although the other two show non-negligible effects, on the production of the p-nuclei at $A \sim 100 - 110$.

6. Variations on the (n,p) reactions on ^{56}Ni (seed nuclei), ^{60}Zn, and ^{64}Ge (first β^+-waiting point on the classical rp-process) show great impact on efficiency of the νp-process. Only a factor of two variation leads to a factor of 10 or more changes in the production of the p-nuclei with $A \sim 100 - 110$ for the first reaction (but somewhat smaller changes for the latter two reactions). This is a consequence that these reactions control the strength of the nuclear flow passing through the (n,p)-waiting points (^{56}Ni, ^{60}Zn, and ^{64}Ge) on the νp-process path.

7. Our result implies that, within possible ranges of uncertainties in supernova dynamics as well as in nuclear reactions, the solar inventory of the light p-nuclei up to $A = 108$ (^{108}Cd) can be attributed to the νp-process, including the most mysterious ones ^{92,94}Mo and ^{96,98}Ru. If highly proton-rich conditions with $Y_{e,3} = 0.60 - 0.65$ are realized in neutrino-driven ejecta, the solar origin of the p-nuclei up to $A = 152$ (^{152}Gd) can be explained by the νp-process.

Our explorations in this study suggest that more refinements both in supernova conditions and in nuclear reactions are needed to elucidate the role of the νp-process as the astrophysical origin of the p-nuclei. In particular, multi-dimensional studies of core-collapse simulations with full neutrino transport, as well as experiment-based rates of the (n,p) reactions on heavy nuclei will be important in the future works.

The project was supported by the Deutsche Forschungsgemeinschaft through Cluster of Excellence EXC 153 “Origin and Structure of the Universe” (http://www.universe-cluster.de).

REFERENCES

Aikawa, M., Arnould, M., Goriely, S., Jorissen, A., & Takahashi, K. 2005, A&A, 441, 1195
Arcones, A., Janka, H. -Th., & Scheck, L. 2006, A&A, 467, 1227
Audi, G., Wapstra, A. H., & Thibault, C. 2003, Nucl. Phys. A, 729, 337
Buras, R., Rampp, M., Janka, H. -Th, & Kifonidis, K. 2006, A&A, 447, 1049
Burrows, A., Hayes, J., Fryxell, B. A. 1995, ApJ, 450, 830
Caughlan, G. R. & Fowler, W. A. 1988, At. Data Nucl. Data Tables, 40, 283
Fischer, T., Whitehouse, S. C., Mezzacappa, A., Thielemann, F. -K., Liebendörfer, M. 2009, arXiv0908.1871
Fröhlich, C., et al. 2006, ApJ, 637, 415
Fröhlich, C., et al. 2006, Phys. Rev. Lett., 96, 142502
Goriely, S., Samyn, M., Pearson, J. M., & Onsi, M. 2005, Nucl. Phys. A, 750, 425
Hayakawa, T., Iwamoto, N., Kajino, T., Shizuma, T., Umeda, H., Nomoto, K. 2008, ApJ, 685, 1089
Hoffman, R. D., Woosley, S. E., Fuller, G. M., & Meyer, B. S. 1996, ApJ, 460, 478
Hüdepohl, L., Müller, B., Janka, H. -Th., Marek, A., Raffelt, G. G 2009, Phys. Rev. Lett., submitted; arXiv0912.0260
Janka, H. -T. & Müller, E. 1995, ApJ, 448, L109
Janka, H. -T. & Müller, E. 1996, A&A, 306, 167
Janka, H. -Th., Buras, R., & Rampp, M. 2003, Nucl. Phys. A, 718, 269
Kitaura, F. S., Janka, H. -Th., & Hillebrandt, W. 2006, A&A, 450, 345
Kuroda, T., Wanajo, S., & Nomoto, K. 2008, ApJ, 672, 1068
Liebendörfer, M., Mezzacappa, A., Messer, O. E. B., Martinez-Pinedo, G., Hix, W. R., & Thielemann, F. -K. 2003, Nucl. Phys. A, 719, 144
Lodders, K. 2003, ApJ, 591, 1220
McLaughlin, G. C., Fuller, G. M., & Wilson, J. R. 1996, ApJ, 472, 440
Meyer, B. S. 1995, ApJ, 449, L55
Meyer, B. S., McLaughlin, G. C., & Fuller G. M. 1998, Phys. Rev. C, 58, 3696
Müller, B., Janka, H. -Th., & Dimmelmeier, H. 2010, ApJS, submitted; arXiv1001.4841

TABLE 1
Results for Various Wind Models

$M_{\rm ns}$ $[M_\odot]$	$\log L_\nu$ [erg s^{-1}]	$r_{\rm wt}$ [100 km]	$Y_{\rm e,9}$[a]	$\dot{M}$ $[10^{-4} M_\odot]$	S $[k_{\rm B}]$	τ_1[b] [ms]	τ_2[c] [ms]	$T_{\rm wt,9}$[d]	$Y_{\rm e,3}$[e]	$Y_{\rm p}/Y_{\rm h}$[f]	$\log f_{\rm max}$[g]	nuc($f_{\rm max}$)[h]	nuc($A_{\rm max}$)[i]
1.4	52.0	3.00	0.600	2.70	57.0	17.5	245	2.19	0.550	124	7.16	^{96}Ru	^{106}Cd
1.4	52.0	1.00	0.600	2.70	57.0	359	1160	5.19	0.509	1.78	4.44	^{64}Zn	^{74}Se
1.4	52.0	2.00	0.600	2.70	57.0	17.5	516	2.95	0.550	124	6.27	^{78}Kr	^{84}Sr
1.4	52.0	2.31	0.600	2.70	57.0	17.5	403	2.65	0.550	124	7.67	^{106}Cd	^{108}Cd
1.4	52.0	3.00	0.600	2.70	57.0	17.5	245	2.19	0.550	124	7.16	^{96}Ru	^{106}Cd
1.4	52.0	4.00	0.600	2.70	57.0	17.5	117	1.80	0.550	124	6.86	^{84}Sr	^{102}Pd
1.4	52.0	5.00	0.600	2.70	57.0	17.5	44.0	1.55	0.550	124	6.69	^{84}Sr	^{84}Sr
1.4	52.0	10.0	0.600	2.70	57.0	17.5	30.0	1.21	0.550	124	6.13	^{78}Kr	^{84}Sr
1.4	52.0	∞	0.600	2.70	57.0	17.5	30.0	—	0.550	124	5.79	^{78}Kr	^{84}Sr
1.4	52.4	8.01	0.600	31.3	33.7	22.8	261	2.19	0.558	42.7	6.00	^{78}Kr	^{84}Sr
1.4	52.2	4.29	0.600	8.66	44.7	18.9	236	2.19	0.554	78.3	6.83	^{84}Sr	^{96}Ru
1.4	52.0	3.00	0.600	2.70	57.0	17.5	245	2.19	0.550	124	7.16	^{96}Ru	^{106}Cd
1.4	51.8	2.22	0.600	0.921	70.1	17.8	262	2.19	0.545	166	7.78	^{102}Pd	^{108}Cd
1.4	51.6	1.71	0.600	0.339	83.3	19.9	301	2.19	0.540	185	7.99	^{106}Cd	^{108}Cd
1.4	51.4	1.37	0.600	0.131	96.3	24.4	371	2.19	0.535	174	8.07	^{106}Cd	^{108}Cd
1.2	52.0	3.27	0.600	3.96	46.8	18.4	241	2.19	0.553	84.4	6.96	^{84}Sr	^{102}Pd
1.4	52.0	3.00	0.600	2.70	57.0	17.5	245	2.19	0.550	124	7.16	^{96}Ru	^{106}Cd
1.6	52.0	2.80	0.600	1.94	68.1	16.4	244	2.19	0.547	178	7.69	^{102}Pd	^{108}Cd
1.8	52.0	2.62	0.600	1.46	80.0	15.4	245	2.19	0.545	243	7.91	^{106}Cd	^{108}Cd
2.0	52.0	2.46	0.600	1.13	93.0	14.4	247	2.19	0.543	335	8.12	^{108}Cd	^{108}Cd
1.4	52.0	3.00	0.550	2.70	57.0	17.5	245	2.19	0.523	42.9	6.25	^{78}Kr	^{84}Sr
1.4	52.0	3.00	0.600	2.70	57.0	17.5	245	2.19	0.550	124	7.16	^{96}Ru	^{106}Cd
1.4	52.0	3.00	0.650	2.70	57.0	17.5	245	2.19	0.576	245	8.14	^{106}Cd	^{108}Cd
1.4	52.0	3.00	0.700	2.70	57.0	17.5	245	2.19	0.603	428	8.34	^{108}Cd	^{120}Te
1.4	52.0	3.00	0.750	2.70	57.0	17.5	245	2.19	0.629	703	8.54	^{138}La	^{138}La
1.4	52.0	3.00	0.800	2.70	57.0	17.5	245	2.19	0.655	1130	8.37	^{138}La	^{152}Gd

[a] $Y_{\rm e}$ at $T_9 = 9$.
[b] time elapsed from $T_9 = 6$ to $T_9 = 3$.
[c] time elapsed from $T_9 = 3$ to $T_9 = 1.5$.
[d] temperature (in units of 10^9 K) just after the wind-termination.
[e] $Y_{\rm e}$ at $T_9 = 3$.
[f] proton-to-seed ratio at $T_9 = 3$.
[g] maximum overproduction factor.
[h] nuclide at $f = f_{\rm max}$.
[i] nuclide at the largest A with $f > f_{\rm max}/10$.

Otsuki, K., Tagoshi, H., Kajino, T., & Wanajo, S. 2000, ApJ, 533, 424
Panov, I. V. & Janka, H. -Th. 2009, A&A, 494, 829
Pruet, J., Hoffman, R. D., Woosley, S. E., Buras, R., & Janka, H. -Th. 2006, ApJ, 644, 1028
Prantzos, N., Hashimoto, M., Rayet, M., & Arnould, M. 1990, A&A, 238, 455
Qian, Y. -Z. & Woosley, S. E. 1996, ApJ, 471, 331
Rayet, M., Arnould, M., Hashimoto, M., Prantzos, N., & Nomoto, K. 1995, A&A, 298, 517
Schatz, H, et al. 2001, Phys. Rev. Lett., 86, 3471
Timmes, F. X. & Swesty, F. D. 2000, ApJS, 126, 501
Wagoner, R. V. 1969, ApJS, 18, 247
Wanajo, S., Kajino, T., Mathews, G. J., & Otsuki, K. 2001, ApJ, 554, 578
Wanajo, S. 2006, ApJ, 647, 1323
Wanajo, S. 2007, ApJ, 666, L77
Wanajo, S., Nomoto, K., Janka, H. -T., Kitaura, F. S., Müller, B. 2009, ApJ, 695, 208
Weber, C., et al. 2008, Phys. Rev. C, 78, 054310
Woosley, S. E., Hartmann, D. H., Hoffman, R. D., & Haxton, W. C. 1990, ApJ, 356, 272
Woosley, S. E., Wilson, J. R., Mathews, G. J., Hoffman, R. D., & Meyer, B. S. 1994, ApJ, 433, 229

TABLE 2
Results for the Changes of Reaction Rates

reaction	factor	$Y_{\rm p}/Y_{\rm h}$[a]	$\log f_{\rm max}$[b]	nuc(f)[c]	nuc(A)[d]	Fig.
standard	1.00	124	7.16	^{96}Ru	^{106}Cd	all
3α	2.00	73.5	6.93	^{84}Sr	^{102}Pd	9
3α	10.0	25.2	6.15	^{78}Kr	^{84}Sr	9
3α	100	10.8	5.26	^{78}Kr	^{80}Kr	9
3α	1/2.00	204	7.67	^{102}Pd	^{108}Cd	9
3α	1/10.0	482	8.04	^{108}Cd	^{108}Cd	9
3α	1/100	719	8.02	^{108}Cd	^{120}Te	9
^{7}Be(α, γ)	2.00	124	7.11	^{96}Ru	^{106}Cd	10
^{7}Be(α, γ)	10.0	122	6.98	^{96}Ru	^{106}Cd	10
^{7}Be(α, γ)	100	117	6.89	^{84}Sr	^{106}Cd	10
^{7}Be(α, γ)	1/2.00	124	7.19	^{96}Ru	^{106}Cd	10
^{7}Be(α, γ)	1/10.0	124	7.24	^{102}Pd	^{106}Cd	10
^{7}Be(α, γ)	1/100	124	7.26	^{102}Pd	^{106}Cd	10
^{10}B(α, p)	2.00	119	7.09	^{96}Ru	^{106}Cd	11
^{10}B(α, p)	10.0	112	6.96	^{96}Ru	^{106}Cd	11
^{10}B(α, p)	100	110	6.92	^{96}Ru	^{106}Cd	11
^{10}B(α, p)	1/2.00	129	7.23	^{102}Pd	^{106}Cd	11
^{10}B(α, p)	1/10.0	135	7.35	^{102}Pd	^{106}Cd	11
^{10}B(α, p)	1/100	138	7.39	^{102}Pd	^{106}Cd	11
^{56}Ni(n, p)	2.00	124	7.01	^{96}Ru	^{106}Cd	12
^{56}Ni(n, p)	10.0	124	7.02	^{84}Sr	^{102}Pd	12
^{56}Ni(n, p)	100	124	7.03	^{84}Sr	^{102}Pd	12
^{56}Ni(n, p)	1/2.00	124	7.45	^{102}Pd	^{106}Cd	12
^{56}Ni(n, p)	1/10.0	124	7.92	^{106}Cd	^{108}Cd	12
^{56}Ni(n, p)	1/100	124	8.01	^{108}Cd	^{113}In	12
^{60}Zn(n, p)	2.00	124	7.15	^{96}Ru	^{106}Cd	13
^{60}Zn(n, p)	10.0	124	7.15	^{96}Ru	^{106}Cd	13
^{60}Zn(n, p)	100	124	7.14	^{96}Ru	^{106}Cd	13
^{60}Zn(n, p)	1/2.00	124	7.22	^{102}Pd	^{106}Cd	13
^{60}Zn(n, p)	1/10.0	124	7.51	^{102}Pd	^{108}Cd	13
^{60}Zn(n, p)	1/100	124	7.69	^{108}Cd	^{108}Cd	13
^{64}Ge(n, p)	2.00	124	7.16	^{96}Ru	^{106}Cd	14
^{64}Ge(n, p)	10.0	124	7.16	^{96}Ru	^{106}Cd	14
^{64}Ge(n, p)	100	124	7.16	^{96}Ru	^{106}Cd	14
^{64}Ge(n, p)	1/2.00	124	7.19	^{102}Pd	^{106}Cd	14
^{64}Ge(n, p)	1/10.0	124	7.41	^{102}Pd	^{108}Cd	14
^{64}Ge(n, p)	1/100	124	7.40	^{106}Cd	^{108}Cd	14

[a] proton-to-seed ratio at $T_9 = 3$.
[b] maximum overproduction factor.
[c] nucleus at $f = f_{\rm max}$.
[d] nucleus at the largest A with $f > f_{\rm max}/10$.

TABLE 3
p-Nuclei Abundances [Si = 10^6] and Their Possible Sources

Species	Abundance[a]	γ-process[b]	ν-process[c]	α-process[d]	νp-process[e]
^{74}Se	0.58	yes	no	yes	yes
^{78}Kr	0.20	yes	no	yes	yes
^{84}Sr	0.13124	yes	no	yes	yes
^{92}Mo	0.386	no	no	yes	yes
^{94}Mo	0.241	no	no	no	yes
^{96}Ru	0.1053	no	no	no	yes
^{98}Ru	0.0355	no	no	no	yes
^{102}Pd	0.0146	no	no	no	yes
^{106}Cd	0.01980	no	no	no	yes
^{108}Cd	0.01410	no	no	no	yes
^{113}In	0.0078	no	no	no	[yes]
^{112}Sn	0.03625	yes	no	no	[yes]
^{114}Sn	0.02460	yes	no	no	[yes]
^{115}Sn	0.01265	no	no	no	[yes]
^{120}Te	0.0046	yes	no	no	[yes]
^{124}Xe	0.00694	yes	no	no	[yes]
^{126}Xe	0.00602	yes	no	no	[yes]
^{130}Ba	0.00460	yes	no	no	[yes]
^{132}Ba	0.00440	yes	no	no	[yes]
^{138}La	0.000397	no	yes	no	[yes]
^{136}Ce	0.00217	yes	no	no	[yes]
^{138}Ce	0.00293	yes	no	no	[yes]
^{144}Sm	0.00781	yes	no	no	[yes]
^{152}Gd	0.00067	no	no	no	[yes]
^{156}Dy	0.000216	yes	no	no	no
^{158}Dy	0.000371	yes	no	no	no
^{162}Er	0.000350	yes	no	no	no
^{164}Er	0.004109	yes	no	no	no
^{168}Yb	0.000323	yes	no	no	no
^{174}Hf	0.000275	yes	no	no	no
^{180}Ta	0.00000258	yes	yes	no	no
^{180}W	0.000153	yes	no	no	no
^{184}Os	0.000133	yes	no	no	no
^{190}Pt	0.000185	yes	no	no	no
^{196}Hg	0.00063	yes	no	no	no

[a] Lodders (2003)
[b] Rayet et al. (1995)
[c] Woosley et al. (1990)
[d] Wanajo et al. (2009)
[e] This work (nuclei indicated by "[yes]" are produced only with $Y_{e,3} > 0.6$)